Materials Research Bulletin 185 (2025) 113291

Contents lists available at ScienceDirect

Materials Research Bulletin

journal homepage: www.elsevier.com/locate/matresbu

Research Papers

Fluorine alkaline earth (MgF_2, CaF_2, SrF_2, BaF_2) influence on thermal, structural, and luminescent properties of Eu^{3+}-doped niobium phospho-fluoride glass

Leandro Olivetti Estevam da Silva [a], V.A.G. Rivera [b], Rodrigo Falci [c], Younès Messaddeq [c], Marcos de Oliveira Junior [b,*], Danilo Manzani [a,*]

[a] São Carlos Institute of Chemistry, University of São Paulo (USP), São Carlos, SP, 13560-970, Brazil
[b] São Carlos Institute of Physics, University of São Paulo (USP), São Carlos, SP, 13560-970, Brazil
[c] Centre d'Optique, Photonique et Laser, Université Laval, Québec, Canada

ARTICLE INFO

Keywords:
Phosphate glass
Alkaline earth metal
Eu^{3+} as optical probe
Solid-state NMR

ABSTRACT

New rare earth-doped glasses with wide transparency and tunable optical properties show promise for various technological applications. While the effects of alkaline earth metals on glass compositions have been widely studied, their role in niobium-phosphate glasses remains unexplored. This study investigates Eu^{3+}-doped niobium-lead pyrophosphate glasses modified with different alkaline earth metals, prepared via melt-quenching. Thermal, structural, optical, and spectroscopic properties were examined. Differential scanning calorimetry (DSC) showed that the thermal stability against crystallization decreased from Mg^{2+} to Ba^{2+}, with Sr^{2+} exhibiting the lowest stability. Raman and solid-state NMR spectroscopy revealed minimal changes in the niobium-phosphate network but shifts in the Q^0/Q^1 phosphate unit ratio were detected. Spectroscopic analysis showed that larger alkaline earth ions increase symmetry around Eu^{3+} and increase the $^5D_0$ lifetime. Sr^{2+}-containing samples showed exceptional results, suggesting a possible substitution between Sr^{2+} and Pb^{2+} due to their similar ionic radii.

1. Introduction

The use of alkaline and alkaline earth metals as glass modifiers have been widely explored in different glass networks, showing several effects on their thermal, structural, and optical properties. Essentially, each alkaline metal can stabilize at least one non-bridging oxygen (NBO) while alkaline earth can stabilize at least two of them, diminishing the connectivity of the phosphate network through P-O-P linkages [1]. Such effects were studied by Guedes et al. [2]. They report that the germanate glass network connectivity, which is directly related to the number of NBOs, depends not only on the amount of metal ions, but also on their atomic radii, affecting the glass transition temperature and thermal stability against devitrification [2]. Kumar et al. studied the influence of different alkaline earth metal oxides in the optical and spectroscopic properties of Eu^{3+} doped fluorophosphate glasses, observing variations in the Eu^{3+} emissions ratio and on the crystal field strength around the ion depending on the modifier [3]. Studies by Yiannopoulos et al. showed how the strength of the M-O bonding (M being alkaline and alkaline earth metals) correlates with some glass properties [4]. For example, they showed that for increasing ionic radii of the metals contained in borate glasses, there is a decrease in the glass transition temperatures, T_g [4]. This effect is caused by the reduction of the glass network connectivity, showing how the cationic charge variation between alkaline and alkaline earth metal is related to a significant variation in the T_g due to the higher crosslinking efficiency of divalent ions [4]. Mercier et al. studied the oxidation–reduction equilibrium of transition metals in phosphate glasses and showed that modifier metals such as alkaline or alkaline earth metals play an important role in controlling the $Cu^{2+}/(Cu^{2+}+Cu^{+})$ ratio due to the difference in the basicity that each modifier metal induces to the glass network, related to the formation of NBO (what increases the basicity and consequently favor the oxidized state) and the polarizability of the oxygen bonded to the metal, affected mainly by the metal's ionic radii [5]. Furthermore, several authors have studied not only the effects caused by the insertion of different alkaline earth metals into different glass compositions (usually using the alkaline earth metal oxides as precursors), but also the so

* Corresponding author.
E-mail addresses: mjunior@ifsc.usp.br (M. Oliveira Junior), dmanzani@usp.br (D. Manzani).

https://doi.org/10.1016/j.materresbull.2024.113291
Received 22 November 2024; Received in revised form 16 December 2024; Accepted 30 December 2024
Available online 31 December 2024

called mixed-modifier effect (MME), exploring how the mixture of different metals can affect properties such as the characteristic temperatures, band gap energy, OH^- content, and many others [6,7]. Although several systematic studies have been made by using different alkaline earth metals to track how they can affect different glass networks, to the best of our knowledge the effects of these metals on the pyrophosphate-niobium glass matrix have not yet been explored.

The binary system $Pb_2P_2O_7$-Nb_2O_5 was first studied by D. Manzani et al., exploring the system for nonlinear optics in photonic applications [8]. They reported the incorporation of up to 60 mol% of Nb_2O_5 in lead-phosphate, obtaining glass samples with good thermal stability against devitrification and increasing glass transition temperatures, as a function of the Nb_2O_5 content. The main feature found for the binary system was the high refractive index of the glasses, making them good candidates for photonics and nonlinear optics, but as promising hosts for rare-earth ions (RE^{3+}) for applications in lightening, energy conversion, solid-state laser, and efficient luminescent materials [8]. As reported, niobium plays the role of either glass former or modifier, depending on the Nb_2O_5 content, inducing structural changes into the main phosphate chain. These changes vary from the formation of NbO_6 octahedral units for up to 40% of niobium oxide — responsible for enhancing the covalent character and increasing the connectivity of the glass structure — to the formation of $[NbO_6]_n$ clusters for up to 60%, leading to a decrease in the crystallization temperature and consequently in the thermal stability against devitrification [8]. Some of the consequences of increasing the niobium oxide content in the binary glasses are the increase in the linear and nonlinear refractive indexes due to the large polarizability of Nb atoms, increasing the transmittance between 200 and 2500 nm, and the increase in the chemical stability of phosphate-based glasses due to the reduction of the hydroxide vibrational band (OH^-), features that make these binary glasses ($Pb_2P_2O_7$-Nb_2O_5) promising matrices to photonic applications [8–10].

In this framework, phosphor fluoride glasses are of great interest when studying optical applications since it merges advantages from both oxide and fluoride glass matrices, marrying the high glass formability, high RE^{3+} solubility and high thermal and mechanical resistance from the phosphate glass with the low phonon energy from the fluoride matrix, which contributes to the reduction of non-radiative decay of RE^{3+} and, consequently, increase their quantum yield [11,12]. In addition, the modification induced by the fluorine to the phosphate network was reported by several studies, combined with the use of alkaline and alkaline earth metals as modifiers of the phosphate glass network by stabilizing the non-bridging oxygens (NBOs) through electrostatic interactions.

Eu^{3+} is an efficient luminescent probe to explore the symmetry around the RE^{3+} as a function of glass composition or after controlled crystallization [13–15]. Eu^{3+} presents some particular spectroscopy properties, as extensively revised by Binnemans [16], in which the transitions $^5D_0 \rightarrow {}^7F_{1,2}$ is useful to provide information about the local symmetry around Eu^{3+}. While the $^5D_0 \rightarrow {}^7F_2$ transition, classified as a hypersensitive transition allowed by induced electric dipole, has its intensity heavily dependent on the symmetry around the ion since it is forbidden for centrosymmetric sites. Moreover, the $^5D_0 \rightarrow {}^7F_1$ transition is classified as a magnetic dipole transition, with a weak intensity unaffected by the environmental symmetry of the Eu^{3+}. In this sense, the intensity ratio R between the $^5D_0 \rightarrow {}^7F_2/{}^5D_0 \rightarrow {}^7F_1$ transitions can be used as a structural optical probe to evaluate the symmetry change resulted from different glass matrices, composition, synthesis conditions, and crystallizations. For instance, D. Wang et al. studied the effect of BaO addition in a germanosilicate matrix by observing a monotonic increase of R from 3.44 to 3.74 when BaO concentration is increased from 5 to 25 mol%, showing that a less symmetrical site is occupied by Eu^{3+} with increase of BaO, which results in stronger luminescent intensities [17,18].

This work presents a thorough and systematic study of a new Eu^{3+}-doped phospho-fluoride glass system, $Pb_2P_2O_7$-Nb_2O_5-XF_2, where X represents Mg^{2+}, Ca^{2+}, Sr^{2+}, and Ba^{2+}. The study explores the effect of alkaline earth ions, considering the periodic variation of their properties such as first ionization energy and ionic radii, within the phosphate-niobium network. Using various structural, thermal, and optical characterization techniques, this new glass matrix was analyzed to understand how alkaline earth ions influence these properties and whether the periodic properties of each metal correlate directly to the observed variations. Additionally, Eu^{3+} was used as a structural optical probe through Judd-Ofelt theory calculations to examine the symmetry changes around the RE^{3+} as a function of the alkaline earth metal.

2. Experimental

Phospho-fluoride glass samples were synthesized by the conventional melt-quenching method with the molar compositions (mol%) $60Pb_2P_2O_7$–$20Nb_2O_5$–$20XF_2$ and $98.5(60Pb_2P_2O_7$–$20Nb_2O_5$–$20XF_2)$:$1.5Eu_2O_3$, X = Mg, Ca, Sr and Ba, labelled as PNX0 and PNXEu, respectively. Lead pyrophosphate was obtained from the decomposition of $PbHPO_4$ through a dehydration reaction at high temperatures following the reaction $2PbHPO_4 \xrightarrow{\Delta} Pb_2P_2O_7 + H_2O$, as described in [19]. The raw materials were stoichiometrically weighed, homogenized in an agate mortar, transferred to a Pt/Au (95/5) crucible, and covered for melting under air at 1100 °C for 40 min. The batch of 10 g of glass was subsequently cast into a pre-heated stainless-steel mold at 400 °C for 2 h to release mechanical tensions followed by slowly cooling to ambient temperature. All samples were polished for optical characterizations.

DSC analyses were performed with a F3 Jupiter Netzsch calorimeter, model STA 449, using a heating rate of 10 °C.min^{-1} under N_2 atmosphere from 400 to 700 C. Raman scattering spectroscopy measurements were recorded with a Jobin-Yvon Horiba-HR800, using a He/Ne laser at 632.8 nm. UV–visible absorption spectra were obtained with a Shimadzu UV-3600 spectrophotometer from 300 to 800 nm. Photoluminescence properties were investigated by excitation, emission, and lifetime spectroscopies for the PNXEu samples with a Horiba Fluorolog 3 equipped with SCD1 detector. Excitation spectra were obtained from 350 to 570 nm by monitoring the emission at 612 nm, while emission spectra were recorded from 455 to 725 nm under excitation at 393 nm. Lifetime values were obtained under 393 nm excitation by monitoring 612 nm emission. In addition, the Judd-Ofelt (JO) parameters were calculated by using standard least-squares method.

Solid state ^{19}F, ^{31}P and ^{207}Pb NMR measurements were performed in an Agilent DD2 spectrometer, operating at 5,64 T and equipped with a 1.6 mm (for ^{19}F and ^{31}P) and a 3.2 mm (for ^{207}Pb and double resonance experiments) Agilent HX probe. The experiments were performed under magic angle spinning (MAS) of 38 and 15 KHz, respectively for ^{19}F and ^{31}P nuclei, while for the ^{207}Pb nuclei the experiment was performed statically. ^{31}P MAS NMR spectra were recorded using 90° pulses of 1.9 μs and a relaxation delay of 300 s. In addition, double-quantum (DQ) filtered spectra were measured using the 1D refocused-INADEQATE sequence [20]. This experiment results in the selective detection of only those ^{31}P nuclei that are involved in a P−O−P linkage ($Q^{(1)}$ and $Q^{(2)}$ units). In contrast, the signals of isolated $Q^{(0)}$ units are suppressed by this pulse sequence. The mixing time for DQ coherence creation was 16.6 ms, corresponding to a value of the indirect spin−spin coupling constant ^2J ($^{31}P-{}^{31}P$) of 30 Hz. Chemical shifts were referenced against an external 85% H_3PO_4 standard. ^{19}F MAS NMR spectra were recorded using the rotor-synchronized Hahn-echo sequence for background suppression, with 90 pulses of 1.4 μs, relaxation delays of 200 s and interpulse delay of 52,6 μs (two rotor cycles). Chemical shifts are reported relative to $CFCl_3$ using solid AlF_3 as a secondary reference (−172 ppm). ^{207}Pb NMR spectra were recorded using the statically Hahn-echo sequence for background suppression with 90 pulses of 3.75 μs and relaxation delays of 20 s. $^{19}F\{^{31}P\}$ and $^{19}F\{^{93}Nb\}$ Rotational Echo Adiabatic Passage Double Resonance (REAPDOR) experiments [52] were carried out using a typical value for ^{19}F π-pulse duration of 8.0 μs and a spinning

frequency of 24.0 kHz. Dipolar recoupling was achieved by ^{31}P or ^{93}Nb pulses applied at a nutation frequency of circa 90 kHz with a duration of 1/3 of the rotor period.

3. Results and discussion

The optical appearance of the PNX0 and PNXEu samples are highly transparent glasses in a homogeneous state and free of strains (see Figure S1). The addition of various alkaline earth metals does not visibly affect the glasses' appearance to the naked eye. However, PNXEu samples exhibit a slight grayish hue compared to the PNX samples. This grayish hue becomes more pronounced from Mg^{2+} to Ba^{2+}, with Ba^{2+} showing the darkest color. This difference in coloration may be attributed to potential, albeit uncontrolled, redox processes occurring between Eu^{3+} and the alkaline earth ions during the melting process.

DSC curves for the PNX0 samples are shown in Fig. 1. The characteristic temperatures, including glass transition (T_g), crystallization onset (T_x) and ionic radii of the alkaline earth metals, are summarized in Table 1. Thermal stability against devitrification, represented as ΔT (the difference between T_x and T_g), is evaluated. Table 1 reveals notable variations in the characteristic temperatures of the samples induced by different alkaline earth metals, particularly in T_x and ΔT. When correlating the ionic radii of the alkaline earth metals with stability against devitrification (ΔT), a discernible trend emerges. An increase in the ionic radii, e.g., from MgF_2 to BaF_2-containing glasses, leads to a decrease in the ΔT value from 141 °C to less than 60 °C. This monotonic decrease in ΔT suggests a periodic substitution of alkaline earth metals within the glass network, wherein larger ions increase the susceptibility to crystallization in the fluorophosphate network and may decrease the coordination number around the cation. For further insights, Fig. 1 also presents the DSC curves for comparison between doped and undoped samples, specifically showing the same characteristic temperatures for PNMg0 and PNMgEu samples. This comparison demonstrates that the introduction of Eu^{3+} at a concentration of 1.5 mol% does not appreciably affect the thermal characteristics of the pristine glass samples. **The addition of RE^{3+}, due to their large ionic radii and high cationic charge, can occasionally induce changes in the characteristic temperatures of a glass. These changes are primarily attributed to distortions in the local environment they occupy and an increase in their coordination number. However, such effects typically occur only at higher concentrations of RE^{3+}. In this case, the characteristic temperatures of the glass remain largely unaffected, primarily due to the low concentration of Eu^{3+} added, which minimally alters the primary composition of the glass matrix. Furthermore, the limited electrostatic interaction between Eu^{3+} and the surrounding atoms in the glass matrix further reduces the structural disruptions.**

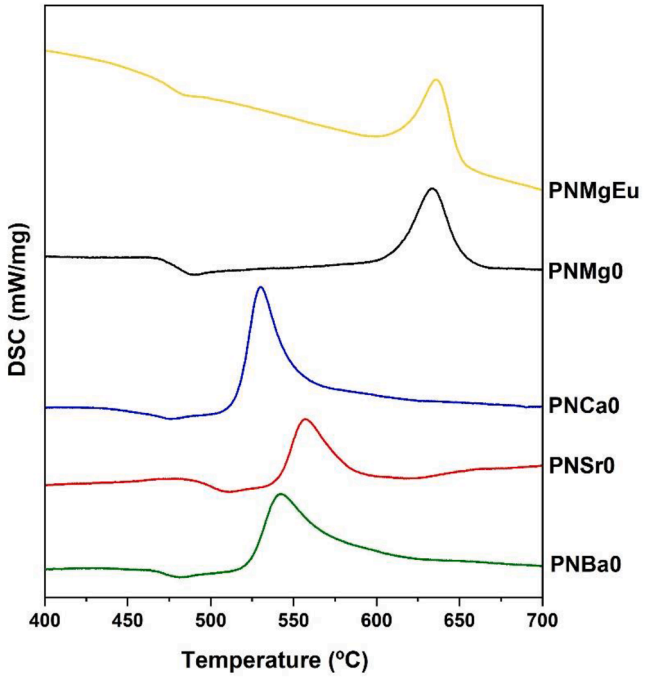

Fig. 1. DSC curves of PNX0 glass samples and comparison with PNXEu sample.

Table 1
Characteristic temperatures, including T_g, T_x and ΔT, and ionic radii of the alkaline earth metals in a hexacoordinated site.

Samples	T_g ± 3 °C	T_x ± 3 °C	ΔT ± 6 °C	Ionic radii (Å)[a]
PNMgEu	470	611	141	0.72 (Mg^{2+}) / 0.947 (Eu^{3+})
PNMg0	470	611	141	0.72 (Mg^{2+})
PNCa0	434	514	80	1.00 (Ca^{2+})
PNSr0	488	540	52	1.18 (Sr^{2+})
PNBa0	466	523	57	1.35 (Ba^{2+})

[a] Ref. [21]

While a consistent monotonic decrease in the ΔT value is evident in samples containing MgF_2, CaF_2 and BaF_2, it is noteworthy that the SrF_2-containing sample deviates from this trend, presenting the lowest ΔT value within the series. This behavior can be attributed to the observed increase in T_g, which is notably higher than that of the other samples, while the T_x shows no significant deviation. Upon analyzing the ionic radii of the constituent elements, a remarkable similarity emerges between the ionic radii of Pb^{2+} (1.19 Å) and Sr^{2+} (1.18 Å), particularly when both are hexacoordinated. This proximity in radii suggests possibility of a substitution between them within the glass matrix. This substitution effect may contribute to observed lower ΔT value, while the increase in T_g can be associated to enhanced network connectivity driven by electrostatic interactions between Sr^{2+} and NBOs sites within the phosphate chains. The deviation observed in the SrF_2-containing sample can be attributed to the significant differences in the ionic radii of other alkaline earth metals, i.e. 0.72 Å for Mg^{2+}, 1.00 Å for Ca^{2+}, and 1.35 Å for Ba^{2+} as hexacoordinated ions [21]. This marked distinction in the ionic radii further highlights the unique behavior exhibited by the sample containing SrF_2.

Fig. 2(a) displays the Raman spectra obtained for all PNX0 glass samples. The spectral pattern observed in all synthesized samples closely resembles those of the previously studied $80Pb_2P_2O_7$–$20Nb_2O_5$ binary system, with all vibrational bands associated with phosphate and niobate bonding [8]. This similarity demonstrates that the addition of 20 mol% of alkaline earth metal fluoride has not introduced any significant differences in the Raman spectra within the analyzed range. Furthermore, comparing the Raman spectra of undoped and Eu^{3+}-doped samples confirm that the addition of 1.5 mol% Eu^{3+} does not cause any discernible changes in the glassy matrix structure. As shown in Fig. 2(b), the spectra only exhibit a broad band around 1530 cm^{-1} due to the fluorescence of the Eu^{3+}, without altering the main phosphate-niobate chain [22]. The main observed bands from the precursor $Pb_2P_2O_7$, at 720, 1013 and 1115 cm^{-1} assigned to the P—O—P linkages in $(P_2O_7)^{4-}$ units, symmetric and anti-symmetric stretching vibration of Q^1 phosphate units, respectively, remains present in the Raman spectra [8]. In addition, strong contributions can be observed centered at 620, 830, 930, and 960 cm^{-1}, attributed to the inclusion of Nb_2O_5 within the pyrophosphate main chain. These peaks correspond to Nb–O short bonds in NbO_6 corner-linked units within a three-dimensional network, Nb–O–Nb bending modes in NbO_6 octahedral units sharing edges and forming chains, Nb–O–Nb in isolated NbO_6 units, and Q^0 symmetric stretching vibrations [8,23,24].

It is important to note that the effects of fluoride addition to the glass composition are not discernible via Raman spectroscopy. As previously reported by D. Monckë and H. Eckert, the characteristic P–F bonding

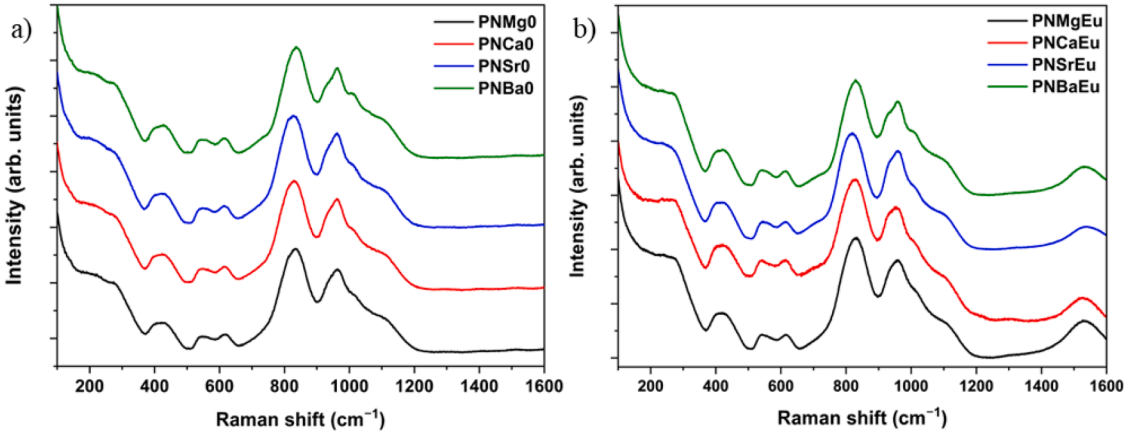

Fig. 2. Normalized Raman spectra of the a) PNX0 and b) PNXEu glass samples (X = Mg^{2+}, Ca^{2+}, Sr^{2+}, Ba^{2+}).

bands appear in the Raman spectra between 700 and 860 cm^{-1} [25]. These bands may overlap with the most intense and broad band observed at 830 cm^{-1}, which is attributed to the insertion of [NbO_6] octahedral units into the phosphate chain [8,25]. When examining the effects of altering the alkaline earth metal in the glasses, Fig. 3 shows the zoomed and deconvoluted region of the spectra where more differences can be observed. The presence of bands at approximately 720 cm^{-1} (band 1), 830 cm^{-1} (band 2), 930 cm^{-1} (band 3), 960 cm^{-1} (band 4), 1013 cm^{-1} (band 5), and 1115 cm^{-1} (band 6) are detectable in all samples, regardless of the glass modifier metal. However, differences in

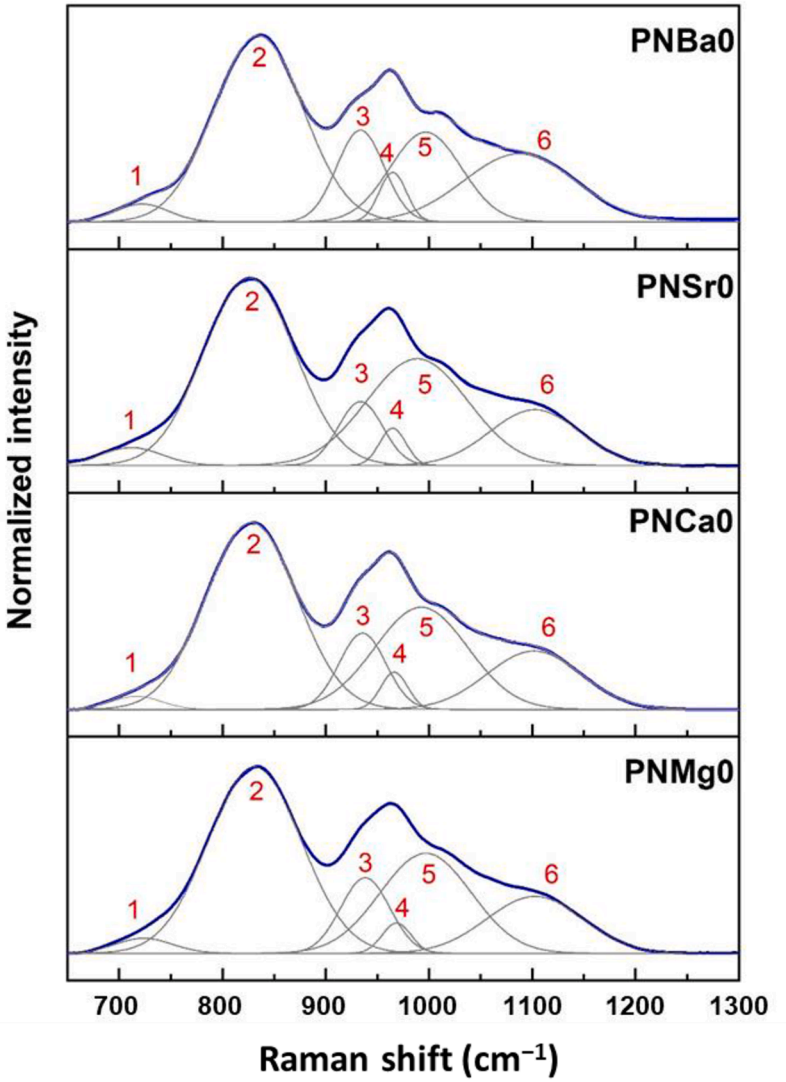

Fig. 3. Deconvolution of the Raman spectra between 650 and 1300 cm^{-1} for PNX0 glass samples.

the integrated area of each band, particularly for bands 3, 5 and 6, indicate that different alkaline earth metals induce small changes in the NbO_6, Q^1, and Q^0 phosphate units. Figure S2 depicts the variation in the absolute area of each band (3, 5, and 6) from the deconvolution shown in Fig. 3. As can be observed, increasing the ionic radii from Mg^{2+} to Sr^{2+} results in a decrease in the intensity of bands 3 and 6 and an increase in the intensity of band 5. Conversely, increasing the ionic radii from Sr^{2+} to Ba^{2+} results in the opposite changes for these bands. By analyzing the assigned bands, it becomes clear that Ba^{2+} enhances the anti-symmetric stretching mode of Q^1 units and the Nb–O–Nb vibrations in isolated NbO_6 units, while it decreases the symmetric stretching of Q^1 units. This indicates that although the variation in alkaline earth metals induces structural changes in the glass matrix in a monotonic manner for the assigned modes in the Raman spectra from Mg^{2+} to Sr^{2+}, there is a threshold for this variation at which the Ba^{2+} exceeds, causing a reversal of these trends, as observed in the variations of each deconvoluted area in Figure S2. More structural details are provided by NMR results described below.

Fig. 4a shows the ^{19}F MAS-NMR spectra of the undoped (PNX0) samples, with their respective deconvolutions. The deconvolution parameters are given in Table 2. Figure S3 shows the comparison of the spectra in Fig. 4 with the ^{19}F MAS spectra of Eu^{3+} doped (PNXEu) samples. There is no appreciable difference between the spectra of doped and undoped samples, revealing that paramagnetic effects on the NMR spectra are negligible at the concentration of 1.5 mol% of Eu^{3+}. On the other hand, the ^{19}F spectra show substantial changes as a function of the alkaline-earth metals. The ^{19}F resonances fall within the range of 100 to -250 ppm but exhibit distinct characteristics depending on the specific alkaline earth metal present. While samples containing Ca^{2+}, Sr^{2+}, and Ba^{2+} exhibit similar spectra, a distinct ^{19}F spectrum is observed for Mg^{2+} containing samples.

Aiming the clarification of the ^{19}F peak attributions, $^{19}F\{^{93}Nb\}$ and $^{19}F\{^{31}P\}$ REAPDOR experiments were performed for the representative samples PNCa0 and PNMg0, which presents spectral features observed for all glasses. For the $^{19}F\{^{31}P\}$ REAPDOR experiment (not shown) we did not observe any dipolar dephasing, even for long evolution times of 1.3 ms. On the other hand, a strong dephasing is observed for the $^{19}F\{^{93}Nb\}$ REAPDOR experiment even for very low evolution times of 182 μs. Fig. 4b shows the comparison between S (with dipolar-recoupling pulse on ^{93}Nb channel) and S_0 (without dipolar-recoupling pulse) signals for the investigated samples, as well as the difference spectrum (ΔS). For the PNCa0 sample it is evident that the REAPDOR effect is less

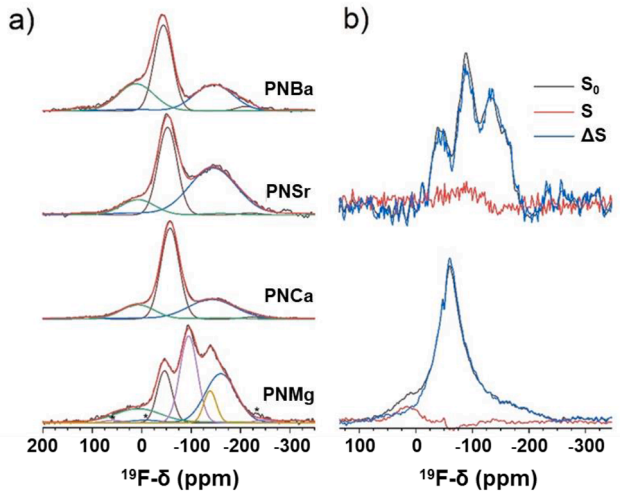

Fig. 4. (a) ^{19}F experimental spectra for the non-doped glass samples PNX0 (X = Mg^{2+}, Ca^{2+}, Sr^{2+} and Ba^{2+}) (black curves) and proposed deconvolutions; (b) $^{19}F\{^{93}Nb\}$ REAPDOR S, S_0 and difference spectra for samples PNCa0 and PNMg0, measured for an echo evolution time (2τ) of 182 μs.

Table 2
Spectral parameters obtained from the simulation of the ^{19}F spectra of samples PNX0, shown in Fig. 4.

Sample	δ_{iso} (± 1 ppm)	Intensity (± 2 %)	FWHM (± 5 ppm)
PNBa0	-146	30	90
	-44	45	45
	11	25	80
PNSr0	-144	50	110
	-52	37	45
	10	13	80
PNCa0	-141	30	110
	-57	53	45
	10	17	80
PNMg0	-160	32	75
	-138	8	30
	-95	31	40
	-46	15	35
	10	14	110

pronounced for the peak at around 10 ppm. From these experiments we can conclude that, except for the sites resonating at 10 ppm, the fluorine environment is dominated by connectivity with Nb species and there is no P-F coordination.

Considering that the F coordination environment is mostly dominated by Nb species, we can attribute the differences observed between spectra to second neighbors or to a mixed coordination environment between Nb and Pb or the alkaline earth. The peak around -150 ppm, its position is unaffected by the alkaline earth species, letting us conclude that this site corresponds to pure F-Nb environments. On the other hand, for Ca^{2+}, Sr^{2+}, and Ba^{2} samples some variation is observed for the central peak, with δ_{iso}values of -57 ppm, -52 ppm, and -44 ppm for samples containing Ca^{2+}, Sr^{2+}, and Ba^{2+}, respectively. The observed upfield shift as a function of alkaline earth is also reported for the chemical shift values of the salts CaF_2 (-108 ppm), SrF_2 (-87.5 ppm), and BaF_2 (-14.3 ppm) [26]. Therefore, we can tentatively assign this resonance to F species in a mixed Nb and alkaline-earth environment. Regarding the peak at 10 ppm, from our experiments did not lead to any evidence that allows a clear attribution. The assignment for this peak remains under investigation.

The significantly different ^{19}F NMR results for the Mg^{2+}-containing glass sample (compared to samples containing Ca^{2+}, Sr^{2+} and Ba^{2+}) can be approached by the previous idea of fluorine ions being more attracted to divalent cations with higher charge to size ratios [27]. This implies that even though the cationic potential (calculated as the ratio between cationic charge and ionic radii) significantly increases between 1.47, 1.72 and 2.00 $Å^{-1}$ (respectively for barium, strontium and calcium), it will only cause deep difference on how fluorine atoms are displaced within the glass matrix for the Mg^{2+}-containing sample, with the highest cationic potential of 2.78 $Å^{-1}$ [21]. The shifting effect of the resonance peaks for lower ppm values was previously revealed by H. Kusumoto et al. [28], when measuring the ^{19}F NMR for aluminosilicate glasses substituting calcium by magnesium in one sample series and strontium by magnesium in other series. $^{19}F\{^{93}Nb\}$ REAPDOR data (Fig. 4b) reveal that also for this sample the F coordination environment is dominated by Nb. Therefore, we can conclude that the multiplicity of peaks observed for the ^{19}F spectrum of this sample reflects a mixed F-Nb/Mg coordination environment which is very complex, hindering any detailed assignments at this time.

^{31}P NMR spectra are depicted in Fig. S4 representing both single pulse and REINAD experiments, while Fig. 5 show the resulting deconvolution on the single pulse experiment based on the REINAD. As previously showed by the ^{19}F NMR experiments, Eu^{3+}-doped glasses show no difference in the spectra compared to the undoped ones, and the same behavior occurred for the ^{31}P NMR experiments, not being relevant to show both undoped and Eu^{3+}-doped samples results again. The black lines on Figure S4 represent the results obtained by the single pulse

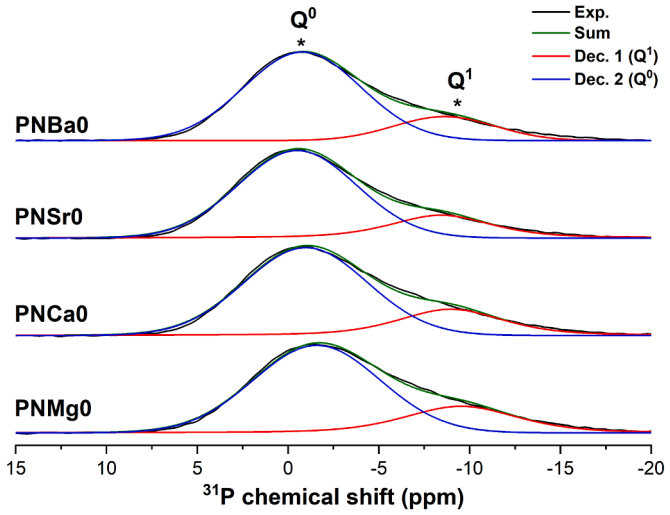

Fig. 5. Deconvolution of the ^{31}P NMR spectra based on the INAD and *onepul* experiments for PNX0 glass samples. Exp. representing the one pulse experiment, Dec.1 and Dec.2 the two deconvoluted peaks and Sum representing the sum of both deconvoluted peaks.

excitation sequence, i.e. the sum of all phosphate groups contribution in only one curve. It can be seen two major contributions for these curves, the most intense centered at -1 ppm and a wide and less intense one at -9 ppm. Aiming for better interpreting which phosphate groups provides these two peaks, DQ-filtered spectra were also acquired using the refocused-INADEQUATE (REINAD), which are represented by blue curves in Figure S4. This experiment is based on the excitation of double-quantum coherences originated from $^{2}J(^{31}P\text{-}^{31}P)$ couplings with the subsequent conversion to single-quantum coherence for observation. Signals from isolated ^{31}P species are eliminated by appropriate phase-cycling. As a result, the ^{31}P spectra thus obtained contain contribution only from phosphate groups that contain P–O–P bonding. As depicted in Figure S4, the less intense peak centered around -9 ppm (from the black curve) is a phosphate group containing P–O–P bonding revealed by the position of the REINAD curve, while the main peak centered at -1 ppm has no P–O–P bonding, showing no response in the REINAD experiment. By fixing the position and width of the peak centered at -9 ppm revealed by REINAD it is possible to adjust the intensity of this peak to the black curve and deconvolute the other contribution at -1 ppm, obtaining two separated peaks by simulating these curves based on the experimental spectra. These simulations are shown in Fig. 5.

By deconvoluting the spectra and conducting simulations, as depicted in Fig. 5, it becomes possible to attribute the peaks to specific phosphate groups. Moreover, results from the REINAD experiments indicate that only the peak centered at -9 ppm can be attributed to phosphate groups containing P–O–P bonding [29]. This clarification simplifies the attribution of the peaks. As observed by the NMR curve evolution, the peak centered at -1 ppm can be attributed to Q^0 units, while the peak at -9 ppm, with lower intensity, is assigned to Q^1 units. The same NMR pattern of these phosphate units is observed varying the alkaline earth fluorides [30].

By calculating the areas related to each peak in the simulated spectra, it is possible to estimate the percentage of each phosphate group in each glass sample. The calculated areas (%) are shown in Table 3. Although the values related to each peak in the ^{31}P NMR spectra do not show a significant change when varying the alkaline earth metal, an increase in the most isolated phosphate group, Q^0, correlates with the increase in the ionic radii of the alkaline earth metal. This observation indicates that while smaller metals have higher cationic potential, larger metals are more capable of promoting the depolymerization of the glass network by increasing the proportion of less connected phosphate groups.

Table 3
Values (in %) of the areas relative to each resonance peak, calculated from the deconvolution depicted in Fig. 5.

Samples	Area (%)	
	Q^0 (-1 ppm)	Q^1 (-9 ppm)
PNMg0	75.7	24.3
PNCa0	76.7	23.3
PNSr0	78.4	21.6
PNBa0	80.9	19.1

Complementarily, ^{207}Pb NMR was performed statically to see whether the Pb nuclei could be coordinated to different species in the different glass matrices, and the results are shown in Figure S5. As it can be seen, regardless of the alkaline earth metal contained in the glass sample, the ^{207}Pb NMR spectra is highly similar to each other, indicating that there's no significant difference in the coordination of these species when altering the glass matrix.

Fig. 6 displays the linear absorption coefficient spectra of the PNX0 and PNXEu glasses, respectively. In Figure 6(a), the undoped glass samples exhibit similar absorption patterns between UV and visible wavelength ranges, without sharp bands associated with electronic transitions. Although the difference in absorbance is not substantial, the spectra indicate a trend where the absorbance of the sample increases as the ionic radii of the alkaline earth ions increase. The absorption spectra acquired for the Eu^{3+}-doped glass samples, as shown in Fig. 6 (b), reveal the emergence of bands within the UV and visible regions, while showing a similar absorption pattern within the analyzed region. **Figure S6 illustrates the electronic transitions of Eu^{3+}, assigned as $^7F_0\rightarrow{}^5D_4$, $^7F_0\rightarrow{}^5G_4$, $^7F_1\rightarrow{}^5G_2$, $^7F_0\rightarrow{}^5L_6$, $^7F_1\rightarrow{}^5L_6$, $^7F_0\rightarrow{}^5D_2$, $^7F_0\rightarrow{}^5D_1$, and $^7F_1\rightarrow{}^5D_1$, centered at 361, 376, 382, 394, 400, 465, 525, and 533 nm, respectively [16, 31]. The weaker emissions at $^7F_0\rightarrow{}^5D_4$, $^7F_0\rightarrow{}^5G_4$, and $^7F_1\rightarrow{}^5G_2$ coincide with the absorption edge of the matrix. The strongest bands, $^7F_0\rightarrow{}^5L_6$ and $^7F_0\rightarrow{}^5D_2$, are electric dipole (ED) transitions and exhibit higher absorption compared to magnetic dipole (MD) transitions like $^7F_0\rightarrow{}^5D_1$ at 525 nm [16, 32]. ED transitions arise from interactions between Eu^{3+} and the electric field of light, which are suppressed in centrosymmetric environments due to the absence of an electric dipole. Though forbidden by Laporte selection rules, ED transitions are relaxed in non-centrosymmetric media [16]. In contrast, MD transitions, allowed by Laporte selection rules, occur due to interactions between Eu^{3+} and the light's magnetic field and are largely independent of symmetry [16]. As lanthanides have inner 4f orbitals with minimal environmental interaction, 4f–4f ED transitions are weak, while MD transitions are even less effective due to reduced magnetic dipole interactions [16].**

The optical energy band gap was determined using absorbance data from UV–Vis-NIR spectroscopy and the absorption coefficient (α), calculated as $\alpha = 2.303 * \left(\frac{A}{d}\right)$, where A is the absorbance and d is the optical path length (1.7 mm glass thickness). This method allows us to determine both the direct and indirect band gap energies for optical transitions in the glasses [33,34]. Both electronic transitions occur near the absorption edge, where electrons in the valence band are excited by photon absorption to the conduction band [35,36]. The indirect and direct optical band gap energy is calculated using the equation $\alpha h\nu = B(h\nu - E_g)^s$, with s = 2 for indirect and s = ½ for direct bandgap, where $h\nu$ is the photon energy (eV), α is the absorption coefficient, B is a constant associated with band tailing, and E_g is the optical band gap energy [37]. To determine the indirect (E_{indir}) and direct (E_{dir}) optical band gap energy, we employed the Tauc plot, which plots $(\alpha h\nu)^{1/2}(eV/cm)^{1/2}$ and $(\alpha h\nu)^2(eV/cm)^2$ versus the photon energy $h\nu$ (eV). Also, by plotting ln(α) versus $h\nu$ it can be obtained the Urbach energy, E_U, for each glass sample. All parameters were calculated as

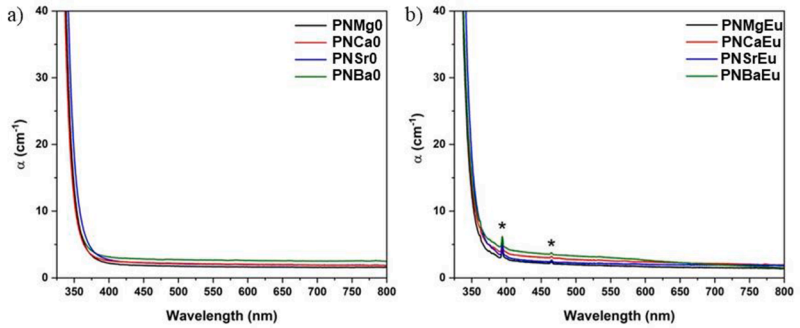

Fig. 6. Linear absorption coefficient spectra of (a) undoped PNX0, and (b) Eu^{3+}-doped PNXEu samples.

demonstrated by S. Hussain et al. [38], fitting the linear part of each plot with a linear regression and obtaining the energy value when y = 0 (see Fig. 7). The calculated energy values for each glass sample are provided in Table 4.

As seen in Table 4, the direct optical bandgap values are higher than the indirect ones for all samples, as expected [33]. While the E_{dir} ranges between 3.57 ~ 3.63, E_{indir} ranges between 3.34 ~ 3.41, showing that the change in the alkaline earth metal — as much as doping with 1.5 mol % of Eu_2O_3 — causes no significant effect on the energy gap between valence and conduction band. Urbach's energy, parameter that gives the width of the localized states and is often used to assess the rate of defects of non-crystalline materials [33,35], also showed a subtly change between different glass samples. Higher values shown by PNMg0 and PNMgEu glasses agrees with other symmetry evaluations, such as R ratio and Ω_2 (next sections). **Small variations in E_{dir}, E_{indir} and E_U with changes in alkaline earth metals and 1.5 mol% Eu_2O_3 doping suggest minimal impact on the optical and electronic properties. The direct and indirect bandgap values, which influence absorption and emission characteristics, exhibit only slight shifts depending on the alkaline earth metals (e.g., magnesium, calcium, strontium, barium) and europium doping [33,35]. Similarly, the Urbach energy, indicative of disorder and tail states in the bandgap, shows limited variation, reflecting minimal changes in structural order and carrier transport properties [33,35]. Overall, the choice of alkaline earth metal and Eu^{3+} doping introduces only subtle modifications to the fundamental energy characteristics of the glasses.**

Table 4
Energy values — indirect bandgap (E_{indir}), direct bandgap (E_{dir}), Urbach energy (E_U) and ΔE (E_{dir} – E_{indir}) — calculated for all PNX0 and PNXEu glass samples.

Parameter (eV)	Glass sample							
	PNX0				PNXEu			
	Mg	Ca	Sr	Ba	Mg	Ca	Sr	Ba
E_{dir} ± 0.01	3.61	3.63	3.58	3.62	3.62	3.59	3.57	3.59
E_{indir} ± 0.01	3.38	3.40	3.34	3.39	3.41	3.38	3.36	3.35
E_U ± 0.01	3.24	3.25	3.18	3.23	3.26	3.21	3.21	3.18
ΔE ± 0.02	0.22	0.23	0.24	0.24	0.21	0.22	0.21	0.24

Different behavior, such as a large difference in these energy values, would be expected when changing the molar composition of the glass (mainly by increasing or decreasing the number of non-bridging oxygens) or using different dopant concentrations, such as shown by S. Hussain et al. and S. Marzouk *et al.* [33,35]. **An example of this effect is demonstrated in a previous study [8], which explores the binary $Pb_2P_2O_7$-Nb_2O_5 system by varying the component concentrations. In that case, increasing Nb_2O_5 from 10 to 60 mol%, significantly alters the covalent character and the number of non-bridging oxygens in the glass matrix, leading to a pronounced decrease in the**

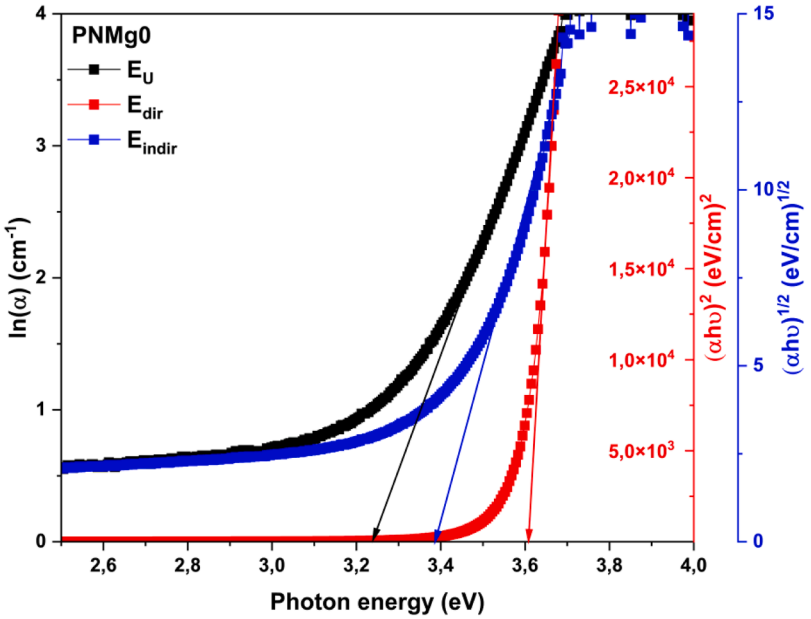

Fig. 7. Tauc plot of ln(***α***), $(\boldsymbol{\alpha h\nu})^2(\boldsymbol{eV/cm})^2$ and $(\boldsymbol{\alpha h\nu})^{1/2}(\boldsymbol{eV/cm})^{1/2}$ versus the phonon energy (eV) to obtain E_U, E_{dir} and E_{indir}, respectively, for PNMg0 glass sample (same method applied for all glass samples).

energy gap value as the conduction and valence bands move closer together.

The luminescent properties of Eu^{3+}-doped glass samples PNXEu were investigated by analyzing their excitation spectra, shown in Fig. 8. These spectra were obtained by monitoring the most intense emission band at 612 nm while recording the excitation intensity across the 350–550 nm range for all glass samples. The high-energy transitions identified in the excitation spectra were assigned as $^7F_0 \rightarrow {}^5D_4$ (361.5 nm), $^7F_1 \rightarrow {}^5D_4$ (365 nm), $^7F_0 \rightarrow {}^5G_2$ (375.5 nm), $^7F_0 \rightarrow {}^5L_7$ (381.5 nm), $^7F_0 \rightarrow {}^5L_6$ (393.5 nm), $^7F_1 \rightarrow {}^5L_6$ (399 nm), $^7F_1 \rightarrow {}^5D_3$ (414 nm), $^7F_0 \rightarrow {}^5D_2$ (464 nm), $^7F_0 \rightarrow {}^5D_1$ (525 nm), and $^7F_1 \rightarrow {}^5D_1$ (532.5 nm). Notably, the $^7F_0 \rightarrow {}^5L_6$ transition at 393 nm exhibited the most intense excitation across all samples, consistent with the expected behavior of Eu^{3+} in glass, which aligns with the absorption spectra shown in Figure 6(b). This Eu^{3+} transition is known for its hypersensitivity to centrosymmetric sites and is allowed by induced electric dipole interactions [16,38]. As the excitation spectra patterns among different PNXEu glass samples showed no substantial deviations, it is challenging to ascertain the influence of different alkaline earth metals on the excitation mechanisms of each sample.

In the excitation spectrum, two lower intensity bands between the $^7F_1 \rightarrow {}^5D_3$ and $^7F_0 \rightarrow {}^5D_2$ transitions, centered at around 426 nm and 443 nm, can be observed. These are denoted as phonon sidebands (PSB) rather than electronic transitions, as shown in Fig. 9 [39]. The appearance of PSB in the excitation spectrum of Eu^{3+} in phosphate glasses is related to the interaction of the lanthanide ions with the vibrational modes (phonons) of the surrounding lattice. In phosphate glasses, Eu^{3+} commonly substitute some of the host cations, and their luminescent behavior is influenced by the local environment provided by the glass matrix. The PSB is associated with vibrational modes coupled to electronic transitions and can be used in conjunction with the $^7F_0 \rightarrow {}^5D_2$ transition, a purely electronic transition (PET), to predict the phonon energy ($\hbar\omega$) of the system.

To obtain the phonon energy, we calculated the energy differences in cm^{-1} between the barycenter of the PSB and PET bands, as shown in Table 5. This table also includes the electron-phonon coupling strength factor (g), which is the ratio of the area associated with the PSB to the area associated with the PET. In our case, the difference between the PET and PSB1 bands is approximately 1025 cm^{-1}, while the difference between the PET and PSB2 bands (or second phonon energy) is about 1900 cm^{-1}. These values indicate that altering the alkaline earth metal in each sample does not significantly affect the phonon energy, as previously suggested by Raman spectroscopy. The first phonon energy value corresponds to the lowest phonon energy observed in phosphates from Raman spectra, typically associated with phosphate glass vibrations related to P–O and $P–O^-$ bonds, which range around 1000–1100 cm^{-1} for all PNXEu samples, specifically the symmetric stretching vibration of Q^1 phosphate units. [40,41]. Additionally, the electron-phonon coupling strength factor reflects the degree of covalency between the Eu^{3+} and its surroundings. The obtained value of approximately 0.025 indicates a high covalent character of the Eu^{3+} site compared to fluorophosphate glasses with lower phosphate concentrations [42] or tellurite glasses [43]. The PSB provides crucial information about the local site symmetry and the structural units surrounding Eu^{3+}, offering valuable experimental data for analyzing non-radiative multiphonon decay processes of Eu^{3+}in glass matrices with varying alkaline earth ions. This includes ions with different ionic radii and electronegativity, particularly those associated with non-bridging oxygens (NBO) in phosphate units.

Given that the most intense excitation, when monitoring the main emission at 612 nm, occurs at 393 nm (assigned to the $^7F_0 \rightarrow {}^5L_6$ transition), and that the primary emissions occur within the visible range, it is crucial to study the multiphonon relaxation events. These events involve transitions from the most populated level, $^5L_6$, to the main emitting level, $^5D_0$, through non-radiative decays. This process has been demonstrated by Miyakawa and Dexter [39,44], it is possible to calculate de multiphonon relaxation rate (W_{mp}) using the following equation:

$$W_{mp} = W_0 e^{-\alpha \Delta E},$$

where α, the host-dependent parameter [39,44], is

$$\alpha = (\hbar\omega)^{-1}\left[ln\left(\frac{p}{g(n+1)}\right) - 1\right],$$

and the parameters p (phonon number) and n (Plank's distribution function) [39,44] are

$$p = \frac{\Delta E}{\hbar\omega}; n = \left(e^{\frac{\hbar\omega}{kT}} - 1\right)^{-1}.$$

In the described equations, W_0 represents the experimental parameter associated with the decay rate at zero energy gap and zero phonon emission [39,44]. The energy gaps (ΔE) for each non-radiative decay

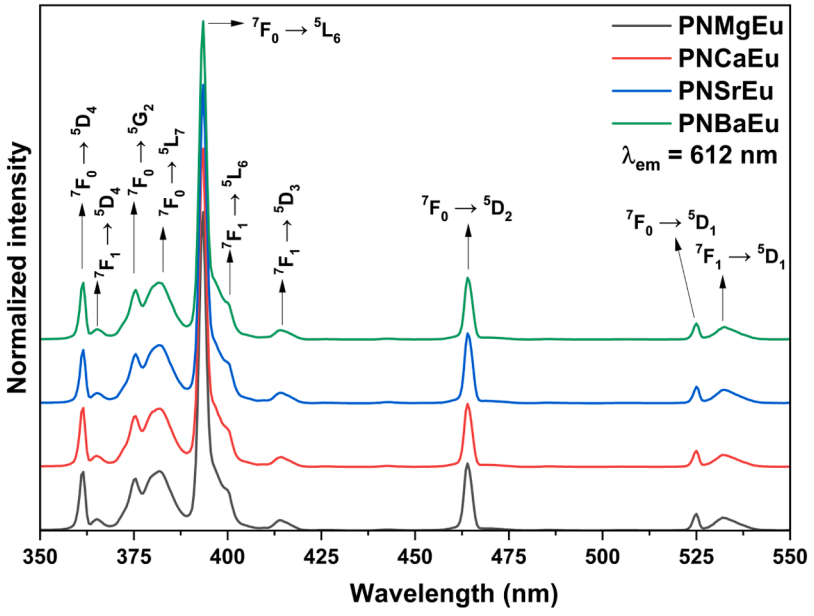

Fig. 8. Normalized excitation spectra of PNXEu glass samples, monitoring the emission at 612 nm and assigning the electronic transitions.

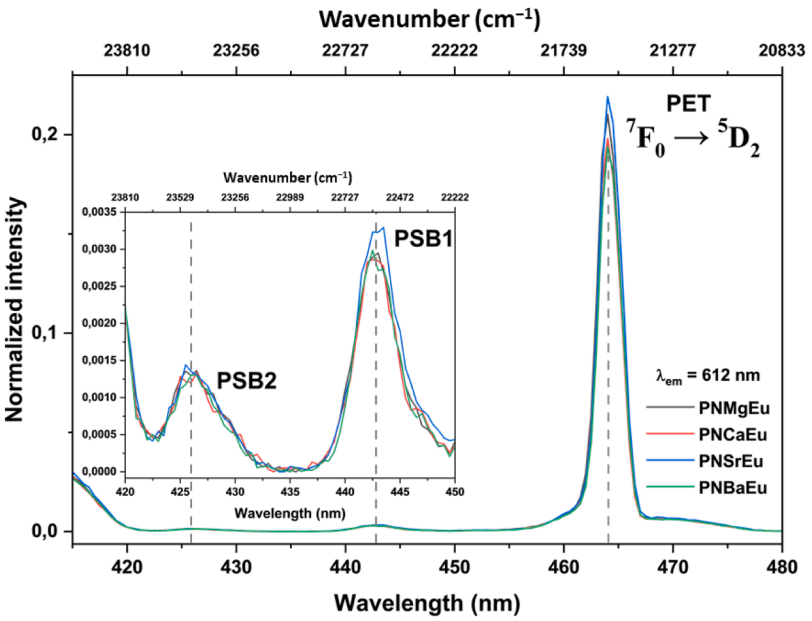

Fig. 9. Vibronic excitation spectra of $^7F_0 \rightarrow {}^5D_2$ transition (PET) of PNXEu glass samples monitoring the emission at 612 nm. Inset: Phonon sidebands (PSB) of PNXEu samples.

Table 5
Calculated values of phonon energy and electron-phonon coupling strength (g) using the barycenter of PET and PSB for each sample.

Sample	PET band (cm^{-1})	PSB band	PSB (cm^{-1})	g	Phonon energy (cm^{-1})
PNMgEu	21,534	1	22,564	0.0243	1029
	-	2	23,432	0.0123	1897
PNCaEu	21,533	1	22,563	0.0254	1028
	-	2	23,431	0.0127	1896
PNSrEu	21,528	1	22,554	0.0262	1019
	-	2	23,432	0.0118	1897
PNBaEu	21,529	1	22,558	0.0257	1024
	-	2	23,436	0.0122	1901

($^5L_6 \rightarrow {}^5D_3$, $^5D_3 \rightarrow {}^5D_2$, $^5D_2 \rightarrow {}^5D_1$, $^5D_1 \rightarrow {}^5D_0$) were obtained from K. Binnemans' review [16], with values of 790, 2890, 2472, and 1746 cm^{-1}, respectively. Using equations these equations and the values obtained for each PET and PSB for each Eu^{3+}-doped glass sample, the multiphonon relaxation rates were calculated and are presented in Table 6.

From Table 6, it can be seen how the W_{mp}/W_0 largely varies in function of different electronic transition, as expected due to the high dependency on the ΔE, once closer energy levels are more expected to occur non-radiative decays. Also, it can be seen how different alkaline-earth metals contained in each glass sample subtly vary the W_{mp}/W_0 values. This occurs because of the high dependency of W_{mp}/W_0 value on the phonon energy ($\hbar\omega$) and on the electron-phonon coupling strength (g). Once these parameters are close to each other, the resulting W_{mp}/W_0 values are also similar. When comparing the obtained W_{mp}/W_0 values with other glass matrices, it can be seen larger differences. As reported by N. Wada [40], all glass matrices (borate, phosphate and silicate) show lower values of W_{mp}/W_0 compared to the present glass samples, mainly because of the electron-phonon coupling strength. The high dependency of W_{mp}/W_0 on g was previously demonstrated by S. Tanabe [41], exploring how the multiphonon relaxation rates increase in phosphate glasses when increasing the g value. When comparing fluoroborate glasses, the present glasses show lower W_{mp}/W_0 values, mainly due to the higher phonon energy of the fluoroborate glasses [39]. Also, as stated by S. Gopi [39], higher values of W_{mp}/W_0 are not expected in systems that depends on the sequential absorption of photons, such as the upconversion, but it helps the excited electrons in higher energy levels (such as $^5L_6$, $^5D_{3,2,1}$) to non-radiatively decay to $^5D_0$ energy level, main radiative emitter on Eu^{3+}.

Table 6
PSB parameters calculated for PSB 1 (at 443 nm) and PSB 2 (at 426 nm) extracted from the excitation spectra for non-radiative decays within the $^5L_6$ and ^5D_J (J = 0, 1, 2 and 3) of Eu^{3+} when the alkaline earth cation is changed in PNXEu (X = Mg, Ca, Sr, Ba) glass samples.

Sample	NR decay	PSB	p	α ($\times 10^{-3}$ cm)	W_{mp}/W_0 ($\times 10^{-2}$)
PNMgEu	$^5D_1 \rightarrow {}^5D_0$	1	1.6955	3.1458	0.4118
		2	0.9199	1.7465	4.7389
	$^5D_2 \rightarrow {}^5D_1$	1	2.4005	3.4834	0.0182
		2	1.3025	1.9297	0.8479
	$^5D_3 \rightarrow {}^5D_2$	1	2.8064	3.6351	0.0027
		2	1.5227	2.0120	0.2983
	$^5L_6 \rightarrow {}^5D_3$	1	0.7671	2.3756	15.3085
		2	0.4162	1.3286	35.0069
PNCaEu	$^5D_1 \rightarrow {}^5D_0$	1	1.6970	3.1058	0.4415
		2	0.9205	1.7322	4.8583
	$^5D_2 \rightarrow {}^5D_1$	1	2.4026	3.4437	0.0201
		2	1.3032	1.9155	0.8780
	$^5D_3 \rightarrow {}^5D_2$	1	2.8089	3.5955	0.0031
		2	1.5236	1.9979	0.3107
	$^5L_6 \rightarrow {}^5D_3$	1	0.7678	2.3350	15.8086
		2	0.4165	1.3141	35.4103
PNSrEu	$^5D_1 \rightarrow {}^5D_0$	1	1.7118	3.1078	0.4399
		2	0.9200	1.7688	4.5581
	$^5D_2 \rightarrow {}^5D_1$	1	2.4236	3.4487	0.0198
		2	1.3025	1.9520	0.8024
	$^5D_3 \rightarrow {}^5D_2$	1	2.8334	3.6019	0.0030
		2	1.5227	2.0343	0.2797
	$^5L_6 \rightarrow {}^5D_3$	1	0.7745	2.3303	15.8666
		2	0.4163	1.3509	34.3965
PNBaEu	$^5D_1 \rightarrow {}^5D_0$	1	1.7045	3.1118	0.4369
		2	0.9181	1.7446	4.7546
	$^5D_2 \rightarrow {}^5D_1$	1	2.4133	3.4513	0.0197
		2	1.2998	1.9274	0.8527
	$^5D_3 \rightarrow {}^5D_2$	1	2.8213	3.6038	0.0030
		2	1.5196	2.0096	0.3005
	$^5L_6 \rightarrow {}^5D_3$	1	0.7712	2.3376	15.7752
		2	0.4154	1.3276	35.0359

Fig. 10 shows the emission spectra of PNXEu glasses, obtained by exciting the samples at the most intense excitation band at 393 nm ($^7F_0$

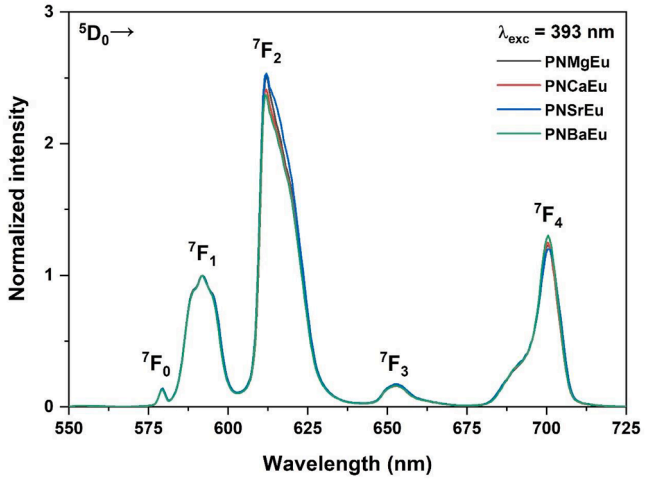

Fig. 10. Emission spectra of PNXEu glass samples normalized by the magnetic dipole $^5D_0 \rightarrow {}^7F_1$ transition, with the excitation at 393 nm.

$\rightarrow {}^5L_6$). Five distinct emission bands were observed, corresponding to the $^5D_0 \rightarrow {}^7F_J$ electronic transitions, where J = 0, 1, 2, 3, and 4. The spectra are normalized to the $^5D_0 \rightarrow {}^7F_1$ magnetic dipole (MD) transition. Due to the high phonon energy of the glass matrices and the narrow energy gaps between the $^5D_{1,2,3}$ states, non-radiative phonon decay from these states to $^5D_0$ is commonly attributed in the literature. Subsequently, radiative decays to the ^7F_J states occur, resulting in emission in the orange to red range [16,38].

Eu^{3+} exhibits distinct dipole characteristics in its $^5D_0 \rightarrow {}^7F_J$ transitions, making the emission spectra a valuable tool for analyzing the symmetry around Eu^{3+}. This analysis is performed by measuring the intensity ratio $R = \frac{^5D_0 \rightarrow {}^7F_2}{^5D_0 \rightarrow {}^7F_1}$ [16]. The $^5D_0 \rightarrow {}^7F_2$ transition is an electric dipole (ED) transition, which is forbidden in centrosymmetric sites due to its null electric dipole moment. In contrast, the $^5D_0 \rightarrow {}^7F_1$ transition is a magnetic dipole (MD) transition and retains its intensity regardless of site symmetry. Therefore, calculating the R ratio for various PNXEu glass samples helps assess whether different alkaline earth metals affect the symmetry of the Eu^{3+} site. Table 7 presents the R values for each glass sample [16].

The R values for each sample indicate that the only notable difference is observed in the glass sample containing Sr^{2+}, while samples containing Mg^{2+}, Ca^{2+}, and Ba^{2+} show minimal variation. This change in the sample with Sr^{2+} suggests that the Eu^{3+} occupies a more asymmetric site in this glass, as evidenced by the higher R ratio. According to A. Varshneya, the presence of alkaline earth metals in interstitial sites within the glass network creates and stabilizes non-bridging oxygens. In our case, the differences among the alkaline earth metals do not induce significant variations in the symmetry and covalency around Eu^{3+} when comparing samples with magnesium, calcium, and strontium, based solely on the R ratio [1]. Although Eu^{3+} is a triply charged ion with a hexacoordinated ionic radius of 95 pm, it is worth noting that Pb^{2+} has a larger ionic radius of 119 pm. [21]. Interestingly, the close values observed for most samples do not apply to the PNSrEu sample, which exhibited the highest R ratio and therefore the lowest network symmetry around Eu^{3+}. This exceptional behavior of the Sr^{2+}-containing sample, compared to other alkaline earth metal-containing samples, suggests that the glass network undergoes structural changes not seen with the other ions. This raises the possibility that Sr^{2+} may be occupying sites typically coordinated by Pb^{2+} in the glass structure, given their similar ionic radii.

Table 7
R of each PNXEu glass considering the area under the curve of the emission spectra and effective ionic radii (IR) of each alkaline earth metal (in pm) [21].

Eu^{3+} transition	PNMgEu	PNCaEu	PNSrEu	PNBaEu
R	2.7303	2.6914	2.8702	2.7070
Ionic radii (pm)	72	100	118	135

Figure S7 displays the lifetime curves of Eu^{3+}, allowing us to analyze the influence of different alkaline earth metals on the lifetime of each PNXEu glass sample. The transition analyzed corresponds to the main excitation and emission bands previously observed, related to the $^7F_0 \rightarrow {}^5L_6$ excitation at 393 nm and the $^5D_0 \rightarrow {}^7F_2$ emission at 612 nm. The decay curves show that the lifetime Eu^{3+} ions are subtly affected by the type of alkaline earth metal used (Mg^{2+}, Ca^{2+}, and Ba^{2+}). Similar lifetime values correlate with the previously calculated $^5D_0 \rightarrow {}^7F_1/{}^5D_0 \rightarrow {}^7F_2$ ratio. The consistent R values for these three metals suggest that the symmetry of the Eu^{3+} site is not significantly influenced by the type of alkaline earth metal, as indicated by both the R ratio and lifetime values. The only notable difference in lifetime across the series of samples with varying alkaline earth metals, consistent with the calculated R ratio values, is observed in the Sr^{2+}-containing sample, which exhibits a lifetime of 1.56 ms while other samples (containing Mg^{2+}, Ca^{2+} and Ba^{2+}) showed a lifetime of approximately 1,67 ms. This lower lifetime supports the hypothesis that substitution of Pb^{2+} with Sr^{2+} may increase local asymmetry around Eu^{3+} in the glass matrix, affecting various properties, including the R ratio and lifetime. Increased asymmetry in the glass matrix raises the likelihood of non-radiative decay, thereby reducing the excited state lifetime [45]. Table 8 compares the lifetimes obtained for other oxide glasses with similar compositions. When compared with lead phosphate glasses, which have a 2:1 PbO to P_2O_5 ratio (like the precursor $Pb_2P_2O_7$ used in this study), the lifetimes of samples synthesized with MgF_2, CaF_2, and BaF_2 are similar. In contrast, the sample synthesized with SrF_2 has a lifetime closer to that of lead phosphate glasses with a 3:1 PbO to P_2O_5 ratio. Additionally, the R ratio values for lead phosphate glasses in the literature, from a 2:1 to a 3:1 PbO to P_2O_5 ratio, increase by approximately 0.12, similar to the change observed in our samples when comparing the use of different fluorides, from 2.70 to 2.83 (Table 6).

The Judd-Ofelt (J-O) theory [47,48] has been used to calculate the three intensity parameters Ω_λ ($\lambda = 2, 4, 6$) evaluating the electric-dipole (ED) transitions of Eu^{3+}. These parameters give information of bonding and local structure in the vicinity of the Eu^{3+} ions. It is important to mention that Ω_2 is related to the covalency of the surrounding O_2, symmetry, and structural changes, while Ω_4 characterize the viscosity, rigidity, and dielectric properties around of the Eu^{3+} ions [49], Here JO parameters Ω_λ, radiative lifetime τ_R and the quantum efficiency $\eta = \frac{\tau_{exp}}{\tau_R}$ of the Eu^{3+} were calculated (see Table 9). Furthermore, Ω_6 remains undetermined due to the inability to experimentally detect the $^5D_0 \rightarrow {}^7F_6$ transition. The minimum Ω_2 value corresponds to the PNBaEu, compared with the other PNXEu, which indicates that the Ba increments the symmetry around the Eu^{3+}, and a decrement of the covalent bonding between Eu^{3+} and its bonds [50]. Contrary to the PNSrEu sample, where the Ω_2 value is higher, i.e., a decrease of the symmetry around the Eu^{3+} and increases the covalent bonding. The asymmetry increment trend

Table 8
Comparison of experimentally obtained lifetime ($^5D_0 \rightarrow {}^7F_2$ electronic transition) for PNXEu samples with other amorphous matrices containing Eu^{3+}.

Glass matrix	τ (ms)	Reference
$98.5[60Pb_2P_2O_7–20Nb_2O_5–20MgF_2]:1.5Eu_2O_3$	1.66	This work
$98.5[60Pb_2P_2O_7–20Nb_2O_5–20CaF_2]:1.5Eu_2O_3$	1.67	This work
$98.5[60Pb_2P_2O_7–20Nb_2O_5–20SrF_2]:1.5Eu_2O_3$	1.56	This work
$98.5[60Pb_2P_2O_7–20Nb_2O_5–20BaF_2]:1.5Eu_2O_3$	1.68	This work
$60PbO–30P_2O_5–9Ga_2O_3–1Eu_2O_3$	1.66	[45]
$67.5PbO–22.5P_2O_5–9Ga_2O_3–1Eu_2O_3$	1.59	[45]
$55.5P_2O_5–14K_2O–6KF–14.5MgO–9Al_2O_3–1Eu_2O_3$	2.54	[3]
$55.5P_2O_5–14K_2O–6KF–14.5SrO–9Al_2O_3–1Eu_2O_3$	2.65	[3]
$55.5P_2O_5–14K_2O–6KF–14.5BaO–9Al_2O_3–1Eu_2O_3$	2.51	[3]
$45P_2O_5–15Nb_2O_3–20BaO–20Na_2O$	1.91	[46]

Table 9
Comparison of experimentally obtained lifetime for PNXEu samples with other amorphous matrices containing Eu^{3+}.

Samples	τ_R (ms)	τ_{exp} (ms)	Ω_2 (10^{-20} cm^2)	Ω_4 (10^{-20} cm^2)	η (%)
PNMgEu	1.99	1.66	4.15	3.44	83
PNCaEu	2.00	1.67	4.09	3.49	83
PNSrEu	1.93	1.56	4.36	3.54	81
PNBaEu	1.97	1.68	4.01	3.62	85

might be assigned to the increase of NBOs inside the glass structure, here, the PNSrEu sample shows a higher increase of the NBO, similar results are also obtained in PSB discussion. On the other hand, Kumar et al. observed that the trend in the J–O parameters ($\Omega_2 > \Omega_4$) corroborated the covalence between Eu^{3+} and ligands, as well as the asymmetry around the metal ion site [51]. Such behavior is also observed in Table 9 for PNXEU samples. Experimental and theoretical lifetime values show the same tendency. Moreover, η describes the radiative emission efficiency of the glass system and the Eu^{3+} at a given wavelength (excitation at 394 nm and emission at 612 nm). In this case, PNBaEu has a higher efficiency compared to the other samples, this is possibly due to the high symmetry of this glass with respect to the others, see Table 9.

4. Conclusions

Based on the previously studied binary based on $Pb_2P_2O_7$-Nb_2O_5, a new glass matrix was obtained with the addition of different alkaline earth metal fluorides as $60Pb_2P_2O_7$–$20Nb_2O_5$–$20XF_2$, with X = Mg, Ca, Sr and Ba, and the effect induced by changing the alkaline earth metals were studied by different thermal, optical, structural and luminescent characterization techniques. DSC measurements revealed that the thermal stability against crystallization significantly shrinks when increasing the ionic radii of the alkaline earth metal contained in the glass, while the sample containing Sr^{2+} showed the lowest value of the series. Structural characterization revealed no changes in the main phospho-niobate chain when altering the alkaline earth metal, but showing a different degree of phosphate unit depolymerization, with more disconnected units when in presence of bigger alkaline earth metals. Eu^{3+} doped glass samples revealed, through luminescent characterization, a higher R ratio value for sample containing Sr^{2+} metal, while for samples containing Mg^{2+}, Ca^{2+} and Ba^{2+} it was shown a similar value, showing that PNSrEu sample showed the highest asymmetry in the Eu^{3+} site of the series. Complementarily, the sample containing Sr^{2+} showed the highest Ω_2 J-O value and the lowest experimental lifetime and quantum efficiency values of the series. The results (and mainly the constant disparity from PNSr sample to the other glasses of the series) suggests that Sr^{2+} ion occupies the Pb^{2+} site in the glass matrix due to their similar ionic radii, causing the glass matrix containing this specific alkaline earth metal to increase its covalent degree, revealed not only by the Eu^{3+} ion used as optical-structural probe (R ratio and J-O parameters) but also by the higher glass transition temperatures and lower optical bandgap. The multiphonon relaxation study revealed a value of ~1025 cm^{-1} as the first phonon energy, which suggests that the highest energy europium's vibronic relaxations are aligned with the symmetric stretching vibrations of Q^1 phosphate units, instead of the anti-symmetric stretching vibration of these units (that shows higher energy of ~1115 cm^{-1}). **Based on the set of results obtained regarding the change of the cation across the alkaline earth metal used, the ionic radius plays a crucial role in controlling the observed physical-chemical and optical properties. Specifically, for the PNX series, the substitution of lead cation sites with strontium causes these samples to deviate from the monotonic behavior observed as the ionic radius increases from Mg to Ba. This study provides a comprehensive investigation of the influence of alkaline earth fluorides on the structural, optical, and luminescent properties of Eu^{3+}-doped phosphate glasses containing Nb_2O_5, unveiling promising materials for applications in optical and photonic systems.**

CRediT authorship contribution statement

Leandro Olivetti Estevam da Silva: Writing – review & editing, Writing – original draft, Visualization, Methodology, Investigation, Formal analysis, Data curation. **V.A.G. Rivera:** Writing – review & editing, Validation, Investigation, Formal analysis. **Rodrigo Falci:** Writing – original draft, Investigation, Data curation. **Younès Messaddeq:** Writing – review & editing, Supervision. **Marcos de Oliveira Junior:** Writing – review & editing, Writing – original draft, Validation, Supervision, Methodology, Investigation, Formal analysis. **Danilo Manzani:** Writing – review & editing, Writing – original draft, Validation, Supervision, Resources, Project administration, Funding acquisition, Formal analysis, Conceptualization.

Declaration of competing interest

The authors declare that they have no known competing financial interests or personal relationships that could have appeared to influence the work reported in this paper.

Acknowledgments

The authors acknowledge grants from São Paulo Research Foundation (FAPESP) (Projects n 2019/16115–8, 2021/08111-2, 2022/01762-0, 2023/05994-6, 2022/02974-1 and 2013/07793-6), and Conselho Nacional de Desenvolvimento Científico e Tecnológico (CNPq) for the financial support (Project n 440225/2021–3, 304718/2023–08 and 312802/2023–4).

Supplementary materials

Supplementary material associated with this article can be found, in the online version, at doi:10.1016/j.materresbull.2024.113291.

Data availability

Data will be made available on request.

References

[1] A.K. Varshneya, Fundamentals of Inorganic Glasses, Elsevier, 2013.
[2] L.F.N. Guedes, L.M. Marcondes, R.O. Evangelista, G. Batista, V.G. Mendoza, F. C. Cassanjes, G.Y. Poirier, Effect of alkaline modifiers on the structural, optical and crystallization properties of niobium germanate glasses and glass-ceramics, Opt. Mater. 105 (2020) 109866.
[3] K.U Kumar, et al., Optical and fluorescence spectroscopy of Eu2O3-doped P2O5–K2O–KF–MO–Al2O3 (M= Mg, Sr and Ba) glasses, Optics Commun. 284 (12) (2011) 2909–2914.
[4] Y.D. Yiannopoulos, GD. Chryssikos, E.I. Kamitsos, Structure and properties of alkaline earth borate glasses, Phys. chemistry of glasses 42 (3) (2001) 164–172.
[5] C. Mercier, et al., A survey of transition-metal-containing phosphate glasses, Comptes Rendus Chimie 5 (11) (2002) 693–703.
[6] K. Griebenow, et al., Mixed-modifier effect in alkaline earth metaphosphate glasses, J. Non-Crystal. Solids 481 (2018) 447–456.
[7] M. Farouk, A. Samir, M. EL Okr, Effect of alkaline earth modifier on the optical and structural properties of Cu2+ doped phosphate glasses as a bandpass filter, Phys. B Condensed Matter 530 (2018) 43–48.
[8] D. Manzani, et al., Highly nonlinear Pb2P2O7-Nb2O5 glasses for optical fiber production, J. Non-Crystal. Solids 443 (2016) 82–90.
[9] Z. Teixeira, O.L. Alves, I.O. Mazali, Structure, thermal behavior, chemical durability, and optical properties of the Na2O–Al2O3–TiO2–Nb2O5–P2O5 glass system, J. Am. Ceramic Soc. 90 (1) (2007) 256–263.
[10] F.F. Sene, J.R. Martinelli, L. Gomes, Optical and structural characterization of rare earth doped niobium phosphate glasses, J. Non-Crystal. Solids 348 (2004) 63–71.
[11] Y. Tian, et al., Engineering rare-earth ions doped fluorophosphate glass for 1.47 μm lasers, J. Non-crystal. Solids 380 (2013) 6–10.
[12] J. Rajagukguk, R. Situmorang, M. Djamal, R. Rajaramakrishna, J. Kaewkhao, P. H. Minh, Structural, spectroscopic and optical gain of Nd3+ doped

fluorophosphate glasses for solid state laser application, J. Luminescence 216 (2019) 116738.
[13] L.A. Bueno, et al., Structural and spectroscopic study of oxyfluoride glasses and glass-ceramics using europium ion as a structural probe, J. Phys. Condensed Matt. 20 (14) (2008) 145201.
[14] L.M. Marcondes, et al., Structural and luminescence characterization of europium-doped niobium germanate glasses and glass-ceramics: Novel insights from 93Nb solid-state NMR spectroscopy, Ceram. Int. (2022).
[15] R. Reisfeld*, E. Zigansky, M. Gaft, Europium probe for estimation of site symmetry in glass films, glasses and crystals, Mol. Phys. 102 (11-12) (2004) 1319–1330.
[16] K. Binnemans, Interpretation of europium (III) spectra, Coord. Chem. Rev. 295 (2015) 1–45.
[17] D. Wang, et al., Effect of BaO on the structure and luminescence properties of Eu3+ doped GSRG glass, J. Non-Crystal. Solids 575 (2022) 121216.
[18] M. Kumar, et al., Probing into structural and spectroscopic properties of Dy3+ doped and Eu3+/Dy3+ co-doped bismuth phosphate (BiPO4) glass ceramics with different modifier fluorides, J. Lum. 245 (2022) 118786.
[19] D. Manzani, et al., Thermal, structural and optical properties of new tungsten lead-pyrophosphate glasses, Opt. Mater. 33 (2011) 1862–1866.
[20] P. Guerry, M.E. Smith, S.P. Brown, 31P MAS Refocused INADEQUATE Spin− Echo (REINE) NMR Spectroscopy: Revealing J Coupling and Chemical Shift Two-Dimensional Correlations in Disordered Solids, J. Am. Chem. Soc. 131 (33) (2009) 11861–11874.
[21] RD. Shannon, Revised effective ionic radii and systematic studies of interatomic distances in halides and chalcogenides, Found. Crystal. 32 (5) (1976) 751–767.
[22] Z. Zhao, et al., Nonlinear optical properties of Eu 2 O 3 doped 5ZnO-20Nb2O5-75TeO2 glasses, Chinese Science Bulletin 49 (2004) 2446–2448.
[23] A. Flambard, et al., Structure and nonlinear optical properties of sodium–niobium phosphate glasses, J. Non-Crystal. Solids 354 (30) (2008) 3540–3547.
[24] A.J. Barbosa, et al., Er3+ doped phosphoniobate glasses and planar waveguides: structural and optical properties, J. Phys. Condensed Matter 20 (28) (2008) 285224.
[25] D. Möncke, H. Eckert, Review on the structural analysis of fluoride-phosphate and fluoro-phosphate glasses, J. Non-Crystal. Solids: X 3 (2019) 100026.
[26] A. Sadoc, et al., NMR parameters in alkali, alkaline earth and rare earth fluorides from first principal calculations, Phys. Chem. Chem. Phys. 13 (41) (2011) 18539–18550.
[27] Q. Zeng, J.F. Stebbins, Fluoride sites in aluminosilicate glasses: high-resolution 19F NMR results, Am. Mineral. 85 (5-6) (2000) 863–867.
[28] H. Kusumoto, et al., Magnesium substitution in calcium and strontium fluoro-phospho-aluminosilicate glasses by multinuclear 19F, 31P, 27Al, and 29Si MAS-NMR spectroscopy, J. Non-Crystal. Solids: X 1 (2019) 100008.
[29] P. Guerry, ME. Smith, S.P. Brown, 31P MAS Refocused INADEQUATE Spin− Echo (REINE) NMR spectroscopy: revealing J coupling and chemical shift two-dimensional correlations in disordered solids, J. Am. Chem. Soc. 131 (33) (2009) 11861–11874.
[30] R.J Kirkpatrick, R.K. Brow, Nuclear magnetic resonance investigation of the structures of phosphate and phosphate-containing glasses: a review, Solid State Nuclear Magnet. Reson. 5 (1) (1995) 9–21.
[31] K. Marimuthu, S. Surendra Babu, G. Muralidharan, S. Arumugam, C.K. Jayasankar, Structural and optical studies of Eu3+ ions in alkali borate glasses, Phys. Status Solidi (a) 206 (1) (2009) 131–139.
[32] S. Selvi, K. Marimuthu, G. Muralidharan, Structural and luminescence studies of Eu3+: TeO2B2O3AOAF2 (A= Pb, Ba, Zn, Cd, Sr) glasses, J. Mol. Struct. 1144 (2017) 290–299.
[33] S. Hussain, et al., Optical investigation of Sm3+ doped in phosphate glass, Glass Phys. Chem. 43 (6) (2017) 538–547.
[34] A.H. Hammad, A.M. Abdelghany, Optical and structural investigations of zinc phosphate glasses containing vanadium ions, J. Non-Crystal. Solids 433 (2016) 14–19.
[35] SY. Marzouk, et al., Linear and non-linear optics and FTIR characteristics of borosilicate glasses doped with gadolinium ions, Opt. Mater. 35 (12) (2013) 2077–2084.
[36] F. Gan Optical and spectroscopic properties of glass. 1992.
[37] SELVI, Structural et al. Structural and luminescence studies on Dy3+ doped lead boro–telluro-phosphate glasses, Phys. B Condensed Matter 454 (2014) 72–81.
[38] K. Linganna, C.K. Jayasankar, Optical properties of Eu3+ ions in phosphate glasses, Spectrochim. Acta Part A Mol. Biomol. Spectr. 97 (2012) 788–797.
[39] S. GOPI, et al., Luminescence and phonon sideband analysis of Eu 3+ doped alkali fluoroborate glasses for red emission applications, J. Mater. Sci. Mater. Electron. 29 (2018) 674–682.
[40] N. Wada, K. Kojima, Glass composition dependence of Eu3+ ion red fluorescence, J. Lum. 126 (1) (2007) 53–62.
[41] S. Damodaraiah, et al., Luminescence behaviour and phonon sideband analysis of europium doped Bi2O3 based phosphate glasses for red emitting device applications, Opt. Mater. 92 (2019) 352–358.
[42] S. Tanabe, K. Hirao, N. Soga, Local structure of rare-earth ions in fluorophosphate glasses by phonon sideband and mössbauer spectroscopy, J. Non-Crystal. Solids 142 (1992) 148–154.
[43] X. JOSEPH, et al., Spectroscopic investigations on Eu3+ ions in Li–K–Zn fluorotellurite glasses, Opt. Mater. 37 (2014) 552–560.
[44] T.;. Miyakawa, D.L. Dexter, Phonon sidebands, multiphonon relaxation of excited states, and phonon-assisted energy transfer between ions in solids, Phys. Rev. B 1 (7) (1970) 2961.
[45] M. Sołtys, et al., Compositional-dependent europium-doped lead phosphate glasses and their spectroscopic properties, Opt. Mater. 40 (2015) 91–96.
[46] J. Wang, et al., Fluorescence properties of trivalent europium doped in various niobate codoped glasses, J. Appl. Phys. 93 (3) (2003) 1482–1486.
[47] BR. Judd, Optical absorption intensities of rare-earth ions, Phys. Rev. 127 (3) (1962) 750.
[48] G.S. Ofelt, Intensities of crystal spectra of rare-earth ions, J. Chem. Phys. 37 (3) (1962) 511–520.
[49] G. Lozano, et al., Cold white light emission in tellurite-zinc glasses doped with Er3+–Yb3+–Tm3+ under 980 nm, J. Lum. 228 (2020) 117538.
[50] N.L.A. Rodin, M.R Sahar, Erbium doped sodium magnesium boro-tellurite glass: Stability and Judd-Ofelt analysis, Mater. Chem. Phys. 216 (2018) 177–185.
[51] M. Kumar, T.K. Seshagiri, S.V. Godbole, Fluorescence lifetime and Judd–Ofelt parameters of Eu3+ doped SrBPO5, Phys. B: Condensed Matter 410 (2013) 141–146.
[52] Y. Ba, H.M. Kao, C.P. Grey, L. Chopin, T. Gullion, Optimizing the ^{13}C-^{14}N REAPDOR NMR Experiment: A Theoretical and Experimental Study, J. Magn. Reson. 133 (1) (1998) 104–114.